Askes, H., Rodríguez-Ferran, A. and Huerta, A., Adaptive analysis of yield line patterns in plates with the Arbitrary Lagrangian-Eulerian method, *Computers and Structures*, Vol. 70, Issue 3, pp. 257-271, 1999

Adaptive analysis of yield line patterns in plates with the arbitrary Lagrangian–Eulerian method

H. Askes[a,*], A. Rodríguez-Ferran[b], A. Huerta[b]

[a] *Delft University of Technology, Department of Civil Engineering, P.O. Box 5048, 2600 GA Delft, The Netherlands*

[b] *Departamento de Matemática Aplicada III, E.T.S. de Ingenieros de Caminos, Universitat Politècnica de Catalunya, Gran Capitán s/n, 08034, Barcelona, Spain*

Abstract

Plasticity models provide suitable tools to describe the so called yield line pattern that occurs with the failure of plates. However, in a Lagrangian description a huge number of finite elements are needed for accurate solutions. Accuracy can be combined with low computer costs by means of the arbitrary Lagrangian Eulerian (ALE) method. With the ALE method, the finite element mesh is automatically refined in the yield lines. A new remesh indicator is proposed that captures newly appearing yield lines as well as already formed yield lines. Numerical examples show the effectiveness of this approach.

Keywords: Plates; Yield lines; Arbitrary Lagrangian Eulerian; Mesh Adaptivity; Remesh indicators

1. Introduction

Plates are widely used in engineering practice, and appear in the floors of buildings, in the foundations of machines or bridge decks, for instance. For the mech anical analysis of plates, the elasticity theory is by now well established, providing theories for both thin and thick plates [1]. When failure involving material nonli nearities is considered, relatively simple plasticity the ories have proven suitable for the analysis of concrete slabs or steel plates [2, 3]. Especially the ideal rigid plasticity assumption with a square yield criterion offers the advantage of analytical upper and lower bounds of the maximum admissible load for a wide range of applications. Furthermore, the yield lines that appear upon plastification can be predicted properly with these analytical methods [2, 3].

However, in general, plates must be considered as a part of a larger structure. Then, analytical methods alone will in general no longer provide suitable and robust tools for failure analyses of the structure as a whole, and numerical approximations must be used. Capturing the yield line pattern can be ensured by using finite element meshes that are sufficiently fine. As a result, computer costs will raise significantly. On the other hand, local refinement or alignment of the mesh according to the yield lines requires that the orien tation of the yield lines is known in advance, which is in general not the case. Therefore, failure analyses are mostly prohibitive for engineering problems. To over come this inconvenience, automatic mesh adaption can be applied. Starting with a coarse finite element mesh, the mesh is adapted *automatically during computation*, such that yield lines are described accurately.

To keep failure analyses of plastic plates robust and cheap (in terms of computer time), we have used the arbitrary Lagrangian Eulerian (ALE) method [4 6] as an automatic mesh adaptivity method. The ALE method is characterised by the fact that material par ticles and the nodes of the mesh are uncoupled, so that nodes can move independently from the material. The total number of degrees of freedom as well as the el ement connectivity remain constant throughout the

* Corresponding author.

calculation, therefore remeshing is only concerned with the determination of the nodal coordinates.

The ALE method has been developed in fluid mechanics [5, 6] to treat fluid structure interaction and large boundary motions [7]. Later, the extension towards nonlinear solids has been made [8]. In forming processes, the ALE method has proven successful [9, 10]. More recently, the extension towards localisation analyses has been made [11, 12]. This approach is also followed here. Remeshing is carried out such that nodes are concentrated in the failure zones. To this end, a new remesh indicator is proposed that starts being effective when yielding is likely to occur, thus anticipating on the formation of the yield lines. The description of the yield zones is therefore improved, while the total number of degrees of freedom remains relatively low.

The paper starts with an overview of plastic analyses of plates, considering both analytical and numerical examples. Then, the implementation of the ALE method is treated briefly. Main issues are the formu lation of a suitable remeshing strategy and the trans port of the state variables after remeshing. Special emphasis is paid to the formulation of a proper remesh indicator. Examples are presented to show the effec tiveness of the ALE method with regard to computer costs and accuracy of the solution.

2. Plastic behaviour of plates

Plasticity theory has successfully been applied to plate structures [2, 3] and enables failure analyses of both concrete slabs and steel plates, for instance. Furthermore, good agreement with experimental results can be obtained [2, 3]. The ideal rigid plasticity assumption together with a square yield criterion (that is, yielding is assumed to take place when the maxi mum in an absolute sense of the bending moments in the principal directions exceeds the plastic bending moment [2, 3]) combines a conceptual simplicity with the availability of analytical upper and lower bounds for the maximum admissible load level. These analyti cal solutions have been treated extensively in the literature [2, 3]. Upper bounds can be obtained by assuming a specific yield line pattern at which a *mech anism* occurs, whereas lower bounds can be derived from an assumption for the distribution of bending and twisting moments at which the structure is in equi librium and where the plastic bending moment is not exceeded. For instance, consider a rectangular plate with aspect ratio $b/a \geq 1$, simply supported on all sides with a uniformly distributed load q (see Fig. 1). Assuming a yield line pattern as shown in Fig. 2, one obtains an upper bound q_{upper} for the load expressed as [2, 3]

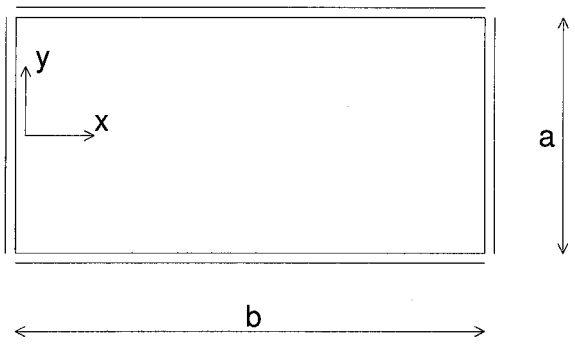

Fig. 1. Rectangular plate, simply supported on all sides, uni form load.

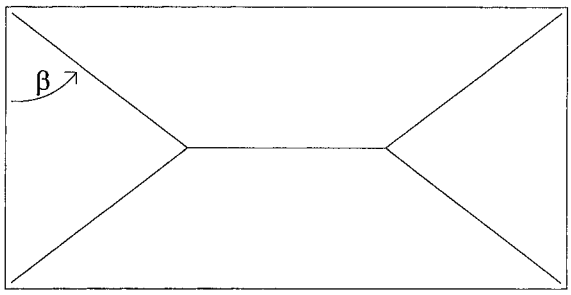

Fig. 2. Yield line pattern.

$$q_{\text{upper}} \quad 8\left(\frac{\frac{b}{a}+\frac{1}{4}\tan\beta}{\frac{b}{a}\quad\frac{1}{3}\tan\beta}\right)\frac{t^2\sigma_y}{3d^2} \tag{1}$$

where β is the angle between the smaller sides and the yield lines departing from the sample's corners (see Fig. 2), t is the thickness of the plate which is assumed to be constant, and σ_y is the yield stress of the material. For a certain aspect ratio, q_{upper} can be found by minimization of Eq. (1) with respect to β. Taking $b \quad 2a$, for instance, leads to $\beta \quad 52^\circ$ and thus $q_{\text{upper}} \quad 3.54\ t^2\sigma_y/a^2$. Assuming a distribution of bend ing moments per unit length m_{ij} as [2, 3]

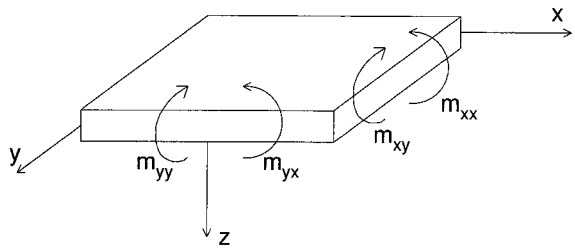

Fig. 3. Sign convention for bending and twisting moments.

$$m_{xx} \quad \frac{t^2\sigma_y}{4a^2}\left(1 \quad 4\frac{x^2}{b^2}\right), \tag{2}$$

$$m_{xy} \quad m_{yx} \quad \frac{t^2\sigma_y}{4a^2}\left(4\frac{x}{b}\frac{y}{a}\right), \tag{3}$$

$$m_{yy} \quad \frac{t^2\sigma_y}{4a^2}\left(1 \quad 4\frac{y^2}{a^2}\right) \tag{4}$$

with m_{ij} as given in Fig. 3, a lower bound q_{lower} for the maximum load can be derived as [2, 3]

$$q_{\text{lower}} \quad 8\left(\frac{a^2}{b^2}+\frac{a}{b}+1\right)\frac{t^2\sigma_y}{4a^2}. \tag{5}$$

Taking again $b \quad 2a$, we obtain $q_{\text{lower}} \quad 3.50\ t^2\sigma_y/a^2$. Obviously, the range between the upper bound and the lower bound is very narrow, so that it can be concluded that the failure behaviour for this plate and for this material model is predicted accurately. An important observation is the dependence of the inclination angle β on the aspect ratio of the sample, which follows from Eq. (1). This angle ranges from 45° for a square plate to 60° for a semi infinite plate. From an engineering point of view it is important to be able to predict the yield line pattern correctly. When using the finite element method instead of analytical methods, it is therefore necessary to use a sufficiently fine mesh, as will be shown by an example.

We have analysed the rectangular plate mentioned above (see Fig. 1) with a uniform load $q \quad 112\ \text{kN/m}^2$. The sizes of the plate read $b \quad 2a \quad 8$ m. The thickness of the plate is $t \quad 0.05$ m. A von Mises yield criterion with isotropic strain hardening has been used. The material parameters are taken as Young's modulus $E \quad 2\times10^8\ \text{kN/m}^2$, Poisson's ratio $v \quad 0.2$, the yield stress $\sigma_y \quad 2\times10^5\ \text{kN/m}^2$ and the hardening modulus $h \quad E/200$. Thus, the applied load equals $q \quad 3.58\ t^2\sigma_y/a^2$. This value deviates slightly from the analytical upper bound, which is due to the different yield criterion and the little hardening that is incorporated. For reasons of symmetry, only the upper left quarter of the plate is considered. The applied element is the so called discrete Kirchhoff triangle (DKT) [1, 13], see also the Appendix. Two updated Lagrangian analyses have been performed, one with 64 elements and one with 1024 elements. The load displacement curves for the two meshes are shown in Fig. 4. The global structural behaviour of the two meshes is the same. However, it can be seen in Figs 5 and 6 that the yield line pattern predicted by the two meshes is different. It is interesting to see that with the finer mesh the same inclination angle of 52° is obtained as with the above mentioned analytical method. Assuming that the finite

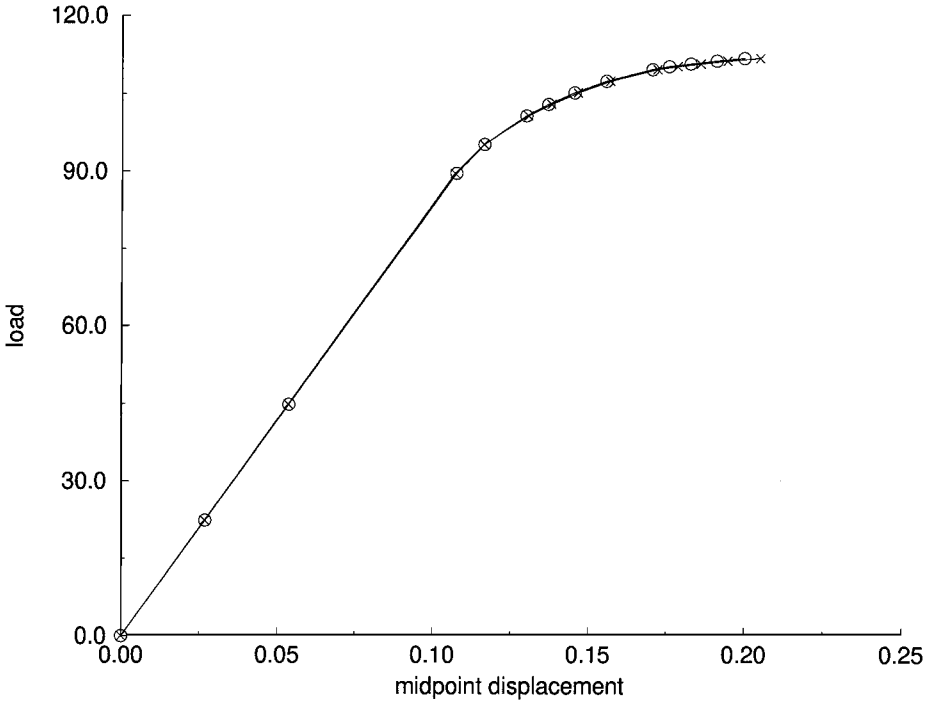

Fig. 4. Load [kN/m^2] vs displacement [m] for the fine mesh × and the coarse mesh ○.

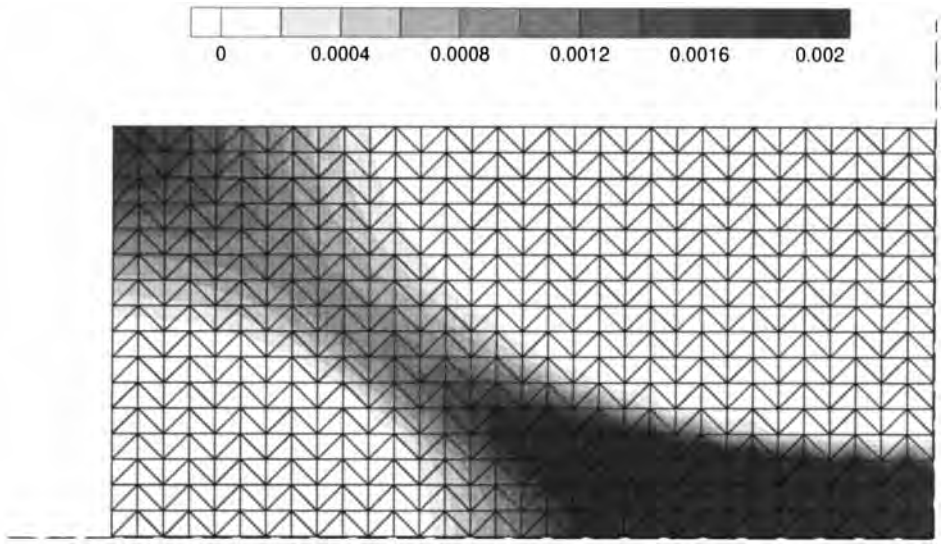

Fig. 5. Contour plot of equivalent plastic strain, fine mesh (dashed lines denote axes of symmetry).

element solution will not change upon further refine ment of the mesh, it can be said that this angle is the exact one. For the coarser mesh the inclination angle is difficult to distinguish. It must be concluded that this mesh is not fine enough for the determination of the yield lines, and a finer mesh must be used to capture the yield line pattern. However, the computational effort involved with the 1024 element mesh is enor mous when compared to the 64 element mesh. To cir cumvent the use of such very fine meshes, we have used the arbitrary Lagrangian Eulerian (ALE) method for the analyses of plates.

3. The ALE method

To be able to describe yield lines with a low number of elements, we detach the nodes of the elements from the material particles. Thus, nodes are able to move independently from the material, and can be

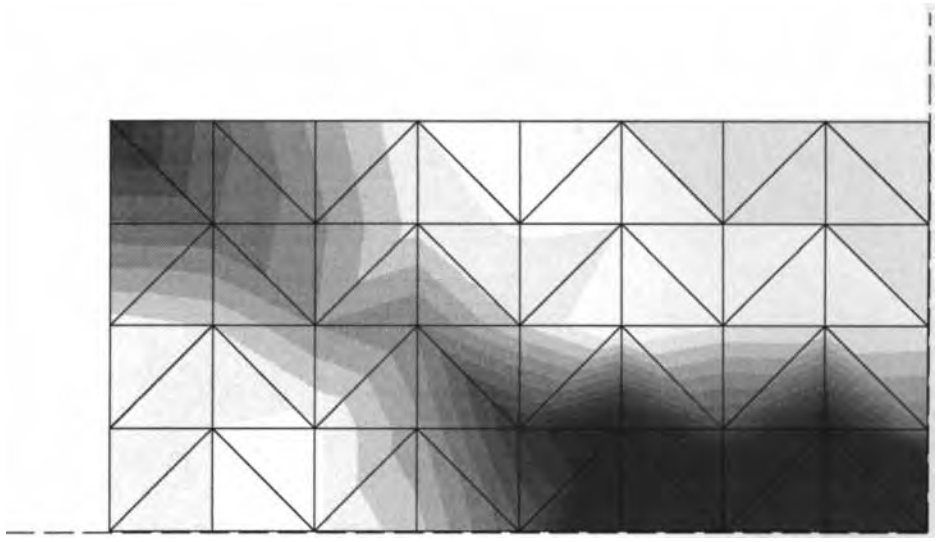

Fig. 6. Contour plot of equivalent plastic strain, coarse mesh (dashed lines denote axes of symmetry).

concentrated in yield lines. Basically, this is an application of the arbitrary Lagrangian Eulerian approach, in which nodes and particles can move independently in space.

Since nodes are no longer attached to particles, this approach is not Lagrangian, and since nodes are not necessarily fixed in space, it is not Eulerian either. While the material motion in space is described in the usual terms of mechanics, a *second, kinematical* framework must be formulated to treat the mesh motion. This leads to the standard ALE equation [5, 6, 12, 14] in which a material property is coupled to a mesh property:

$$\left.\frac{\partial f}{\partial t}\right|_{x} \quad \left.\frac{\partial f}{\partial t}\right|_{\chi} + c_j \frac{\partial f}{\partial x_j} \tag{6}$$

where X denotes a material particle and χ denotes a node. The notation $|_a$ means "keeping a fixed". In Eq. (6), x_j are the spatial coordinates, while c_j are the components of the so called convective velocity, which is the relative velocity of the material with respect to the mesh:

$$c_j \quad \left.\frac{\partial x_j}{\partial t}\right|_{x} \quad \left.\frac{\partial x_j}{\partial t}\right|_{\chi}. \tag{7}$$

In the current implementation, only small deformations are considered, so that the first term on the right hand side of Eq. (7) cancels. The second term in Eq. (7) denotes the mesh velocity, which is set by the mesh displacement. In fact, c is never computed in our implementation: only the mesh incremental displacements are calculated. These mesh displacements follow from the *remeshing strategy*. The remeshing strategy determines in which zones nodes should be concentrated, and in which zones elements are allowed to remain large. The remeshing is carried out in two steps. Firstly, a remesh indicator is computed. This remesh indicator, which is denoted K, takes large values in zones where elements should be small and vice versa. Secondly, the remesh indicator is equidistributed over the whole domain, that is, the product of element size times remesh indicator must yield the same value for each element:

$$K_i \times \Omega_i \quad K_j \times \Omega_j \quad \forall i,\ j \tag{8}$$

where i and j denote element numbers and Ω represents the element size. Eq. (8) can be translated to [11]

$$\frac{\partial}{\partial \chi_i}\left(K \frac{\partial x_j}{\partial \chi_i}\right) \quad 0 \tag{9}$$

which can be solved by applying a Galerkin's variational principle, e.g. [12, 15]. Together with a suitable definition of the remesh indicator, Eq. (9) fully determines the mesh displacement. Formulation of the remesh indicator will be topic of the next section.

From Eq. (6) it can be seen that the convective velocity c and, thus, the mesh incremental displacement, appears when time derivatives of f are involved. Within a quasistatic nonlinear framework, which is chosen here, these convective terms only appear in the constitutive relations [16] (on the other hand, if a *transient* analysis is carried out convective terms also appear in the equations of motion [12, 16]). For nonlinear materials, stresses and strains are history dependent, that is, stress and strain fields are not only determined by displacement (and/or temperature) fields, but also by the previous states. Since history is stored in the material particles and integration points are related to the mesh, convective terms appear in the constitutive update. This follows from applying Eq. (6) on the general constitutive update:

$$\left.\frac{\partial \eta}{\partial t}\right|_{x} \quad \left.\frac{\partial \eta}{\partial t}\right|_{\chi} + c_i \frac{\partial \eta}{\partial x_i} \quad \phi(\eta) \tag{10}$$

where η is a stress component or a state variable, and ϕ is a general term given by the constitutive equations. Note that ϕ is a function of η, which emanates from the nonlinear material behaviour. From Eq. (10) it can be seen that spatial derivatives have appeared through the ALE formulation, which is due to the fact that integration points do not always coincide with the same material particles throughout the computation.

We have applied a split step algorithm [16, 17] to solve Eq. (10). Firstly, the stresses and the state variables are updated at a material level, that is, no convection is taken into account and the constitutive update is in fact fully Lagrangian. This results in an intermediate value of η, denoted η^{L}, which is updated in time but evaluated at material particles that no longer coincide with the integration points. Therefore, the first step of the update from time t up to time $t + \Delta t$ reads

$$\eta^{\mathrm{L}} \quad \eta_{(t)} + \phi \Delta t. \tag{11}$$

Secondly, η^{L} is transported from the integration points of the mesh before remeshing towards the (same) integration points of the mesh after remeshing. In this stage, no time integration is involved but pure convection is considered. The first step is the same as the constitutive update in a standard Lagrangian finite element algorithm. Therefore, only the second, *transport* stage has to be added to a finite element algorithm. We have used the Godunov method [14 18] to perform the transport of the stresses and the state variables. This method is especially suitable for the transport of piecewise constant fields, which is exactly the case in finite elements with piecewise linear displacement fields and constant stress and strain fields.

However, an extension towards higher order elements has been made [17], which has proven to give accurate results. The basic idea is to consider an element with multiple integration points as a configuration of *subele ments*, each sub element being the domain of exactly one integration point (see Fig. 7). Within a sub el ement, η is assumed to be constant. The Godunov method for the transport of η at each integration point then reads [15 17]

$$\eta_{(t+\Delta t)} \quad \eta^{\mathrm{L}} + \frac{1}{2\Omega}\sum_{\Gamma\ 1}^{N} F_{\Gamma}(\eta^{\mathrm{L}} \quad \eta_{a}^{\mathrm{L}})[1 \quad \mathrm{sign}(F_{\Gamma})] \qquad (12)$$

where Ω is the volume of the considered sub element, N is the number of sides of the sub element, the sub script a in η denote the value of η in an adjacent sub element, and F_{Γ} at side Γ is given by

$$F_{\Gamma} \quad \int_{\Gamma} \Delta x_i|_{\chi} n_i \, \mathrm{d}\Gamma \qquad (13)$$

with $\Delta x\big|_{\chi}$ the mesh incremental displacement and n_i the components of the outward normal to side Γ. The presented formalism for the transport is applicable to every element type in which sub elements can be ident ified. For the DKT element, which is used in the cur rent study, this results in both transport between sub elements of the same element as well as transport between sub elements of adjacent elements. More specifically, two so called *internal* transports have to be carried out, as well as one *external* transport in case an adjacent element exists. For instance, consider sub element A of the right element in Fig. 8. Internal trans port is carried out between sub elements A and B and between sub elements A and C, whereas external trans port takes place between A and sub element E of the left element.

Provided that a formulation of the remesh indicator is given, the ALE framework is completed through Eqs. (9) and (12), and can be added to a finite element algorithm.

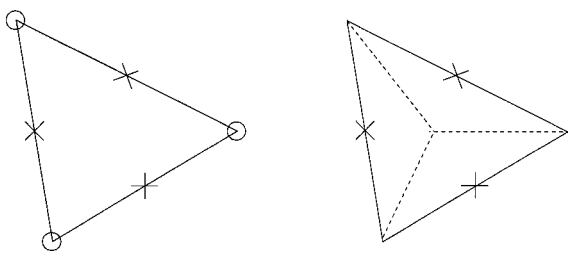

Fig. 7. The DKT element, nodes ○ and integration points × (left), and subdivision for use of Godunov method (right).

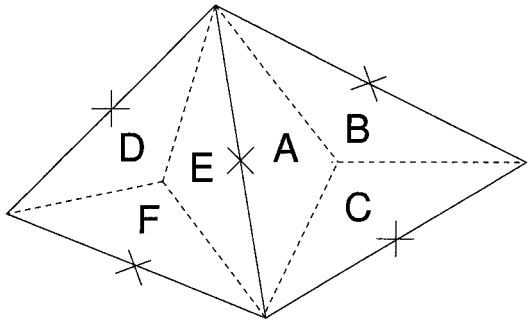

Fig. 8. Transport between integration points.

4. Formulation of the remesh indicator

The crucial question is, therefore, in which zones the elements must be concentrated. Inherent in our pro blem statement, which is the analysis of yield patterns in plates, small elements are needed in the yield lines. Furthermore, it is preferable to have small elements in zones which are close to plastification, since excessively large elements may delay the onset of plastification. In other words, the finite element mesh should be able to *anticipate* the formation of new yield lines, as well as to describe present yield lines accurately. Thus, remeshing is carried out in both the elastic and the plastic stage of the analysis. We have translated this into the following criteria for the remesh indicator:

1. Integration points that are not plastified and that are not "likely at all" to plastify are assigned a pre defined minimum value of the remesh indicator.
2. Integration points that are at the point of plastifica tion are assigned a predefined fraction of the maxi mum possible value of the remesh indicator.
3. Integration points that undergo plastic deformations are assigned a larger value of the remesh indicator than the elastic integration points, and the larger the plastic deformation, the larger the value of the remesh indictor.
4. The remesh indicator should be continuously depen dent on the state variables. Specifically, this means that the value of the remesh indicator at the end of the elastic stage is equal to the value of the remesh indicator at the beginning of the plastic stage.

With a remesh indicator that obeys these criteria, remeshing can be carried out. In a remeshing process, one can distinguish between *direction* and *magnitude*. The former tells to which zones nodes should move, while the latter indicates to which extent this node should move in this direction. In order to uncouple *magnitude* and *direction* of remeshing, we have used the following definition of K [11, 12, 15]:

$$K \quad aR + 1 \tag{14}$$

where a is a parameter that adjusts the magnitude of the remeshing process with respect to variations of R over the domain, and R determines the direc tion of remeshing. The term 1 on the right hand side is added to avoid numerical problems that may arise through ill conditioning of Eq. (9) when $K \quad 0$. The parameter R depends on the state variables. The definition of R is such that R varies between 0 and 1, where low values of R correspond to low desired mesh densities and high values of R account for large mesh densities. Since $0 \leq R \leq 1$, the following inequalities hold: $1 \leq K \leq a + 1$. Equidistribution then leads to a ratio of maximum element size over minimum element size equal to $a + 1/1$ for the one dimensional case [11, 12]. This can be understood by considering that equidistribution of the remesh indi cator is equivalent to requiring that K times element size yields the same value for each element [cf. Eq. (8)].

The criteria for the remesh indicator formulated above are now imposed on the definition of R, since R drives the direction of the remeshing process. The definition of R must be suitable for the prediction of newly appearing yield lines as well as for the description of the already formed yield lines. Therefore, we distinguish between integration points that are purely elastic and integration points that have plastified.

For elastic integration points R ranges between 0 and α ($0 \leq \alpha \leq 1$), whereas R takes values between α and 1 for plastic integration points. α is a parameter that determines how much of the remeshing should be carried out in the elastic stage. In other words, for a given value of a, α determines the element size at the onset of plastification.

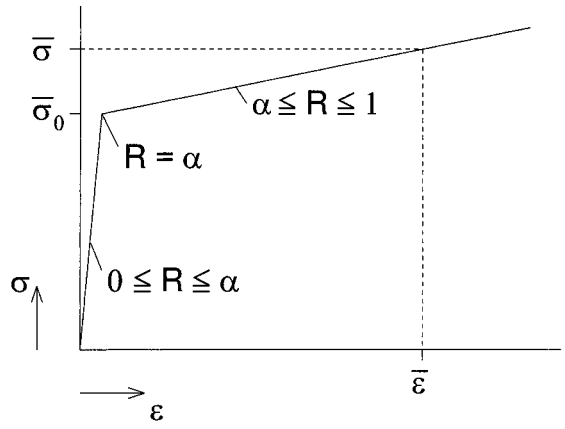

Fig. 9. Hardening curve.

For each integration point, R is defined as

$$\text{if purely elastic} \quad R \quad \alpha \frac{\sigma_{eq}}{\bar{\sigma}_0} \tag{15}$$

$$\text{else} \quad R \quad 1 \quad (1 \quad \alpha) \frac{\bar{\sigma}}{E\bar{\epsilon}} \tag{16}$$

where $\sigma_{eq} \quad \sqrt{3J_2}$ is the equivalent stress with J_2 the second invariant of the deviatoric stress tensor, $\bar{\sigma}$ is the current yield stress, $\bar{\sigma}_0$ is the initial yield stress, and $\bar{\epsilon}$ is the equivalent total strain associated with $\bar{\sigma}$ [see Fig. 9]. Note that non generalised stresses are used in Eqs. (15) and (16), whereas most finite element packages use generalised stresses for plate elements.

Eq. (15) can be understood by considering that the yield function in von Mises plasticity is stated as $\sigma_{eq} \quad \bar{\sigma} \leq 0$. Therefore, the ratio $\sigma_{eq}/\bar{\sigma}_0$ denotes how close an integration point is to yielding. The $\bar{\sigma}/E\bar{\epsilon}$ fac tor in Eq. (16) denotes the ratio of the secant stiffness over the initial stiffness, and gives information on the amount of plastic strain with respect to the total strain [15].

Hence, two parameters have appeared that deter mine the magnitude of the remeshing process, namely a and α. The parameter a sets the maximum possible element size over the minimum possible element size. Through α, the ratio of the minimum possible element size in the elastic regime over the minimum possible el ement size in the plastic region is set. Our numerical tests indicate that taking $\alpha \approx 0.2$ gives the best results.

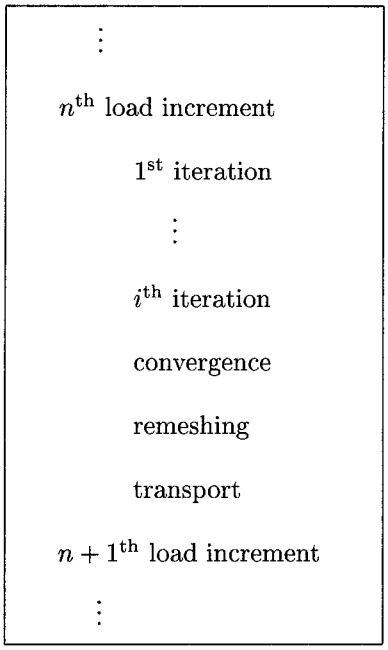

Fig. 10. Remeshing and transport added to a finite element al gorithm.

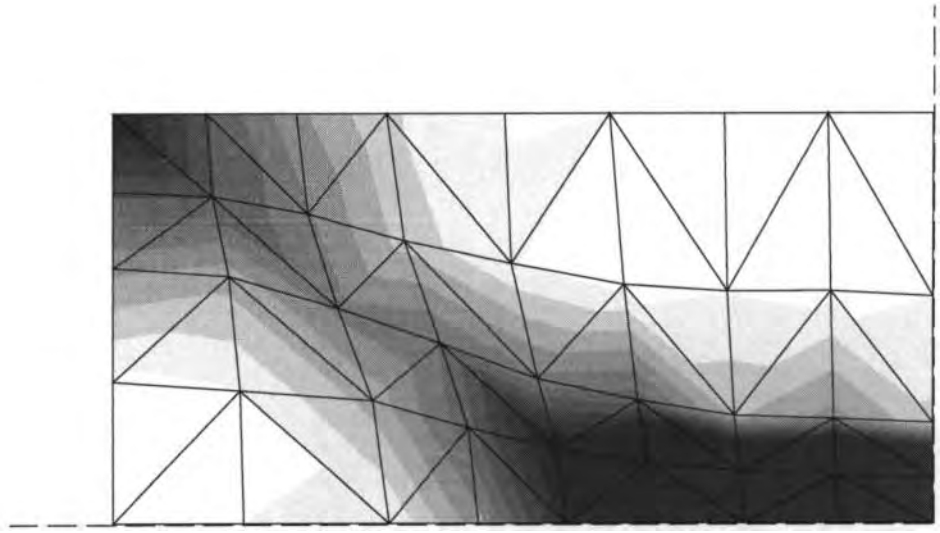

Fig. 11. Contour plot of equivalent plastic strain, ALE mesh (dashed lines denote axes of symmetry).

Estimation of the parameter a can be done when considering Eq. (8). The remesh indicator K is assumed to be constant within each element. We desire a certain element size Ω_{des} for a certain value K_{des}. The values for K_{des} and Ω_{des} usually follow from the material model; see Eqs. (15), (16) and Refs. [19, 20], respectively. According to Eq. (8) it holds that $K_{des} \times \Omega_{des} \quad K_{min} \times \Omega_{max}$, where Ω_{max} is the element size for the minimum value of K. In this study, $K_{min} \quad 1$ [cf. Eq. (14)]. The value for Ω_{max} is not known in advance, but in the case of a uniform initial mesh $\Omega_{max} > \Omega_{init}$. It can then be written that [21, 22]

$$\frac{K_{des}}{1} \quad \frac{\Omega_{max}}{\Omega_{des}} > \frac{\Omega_{init}}{\Omega_{des}} \tag{17}$$

from which a value for a can be extracted. The ratio between Ω_{max} and Ω_{init} depends on how many elements are drawn towards the yield lines. If this number is relatively high, then the number of elements that have to cover the remainder of the domain is relatively low, and Ω_{max} will be significantly higher than Ω_{init}. On the other hand, the difference is less pronounced if a relatively low number of elements is concentrated in the yield lines.

5. Examples

To test the effectiveness of the framework developed above we have implemented the ALE method in the object oriented finite element code Castem2000 [23]. Remeshing and transport are executed consecutively at the end of each load increment (see the algorithm shown in Fig. 10).

5.1. Rectangular plate

As a first example, the rectangular plate of Section 2 has been analysed. The same finite element configuration and the same material set as the coarser mesh from Section 2 has been used. We desire an approximate element size $\Omega_{des} \quad 0.04\,m^2$ for a value of the equivalent plastic strain $\epsilon_{pl} \quad 0.001$. Since the initial element size equals $0.125\,m^2$, Eq. (17) results in an approximate lower bound for the remesh parameter a as $a > 3.1$, where $\alpha \quad 0.2$ has been taken. Since the plastifying part of the domain is relatively large, it is expected that Ω_{max} is substantially larger than Ω_{init}. Therefore, we have taken $a \quad 14$. Again, only one quarter of the plate has been analysed. In Fig. 11 a

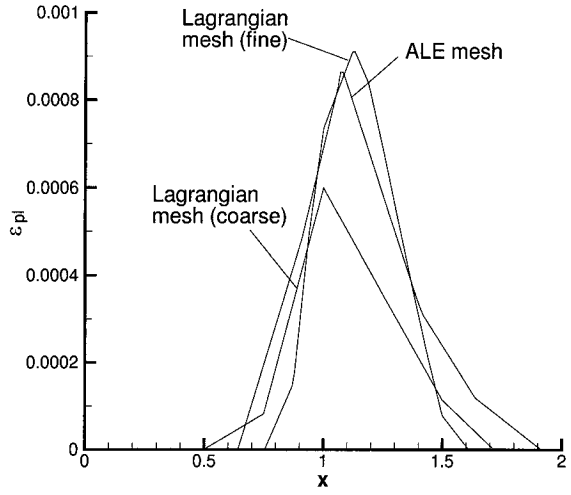

Fig. 12. Profiles of equivalent plastic strain along $y \quad x$.

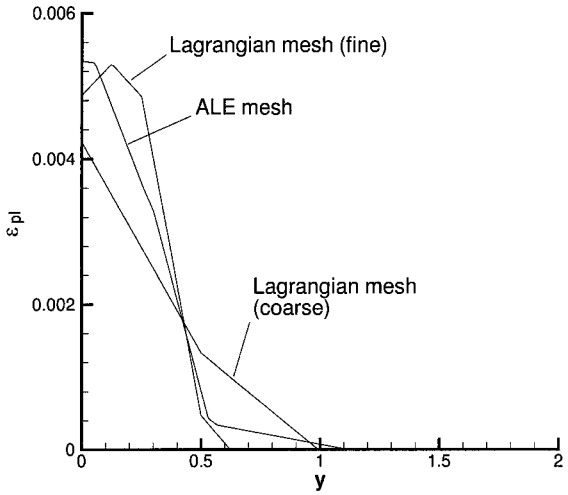

Fig. 13. Profiles of equivalent plastic strain along x 3.

contour plot of the equivalent plastic strain is depicted. Comparison with Fig. 5 shows that basically the same yield line pattern as with the fine Lagrangian mesh is predicted with the ALE analysis. On the other hand,

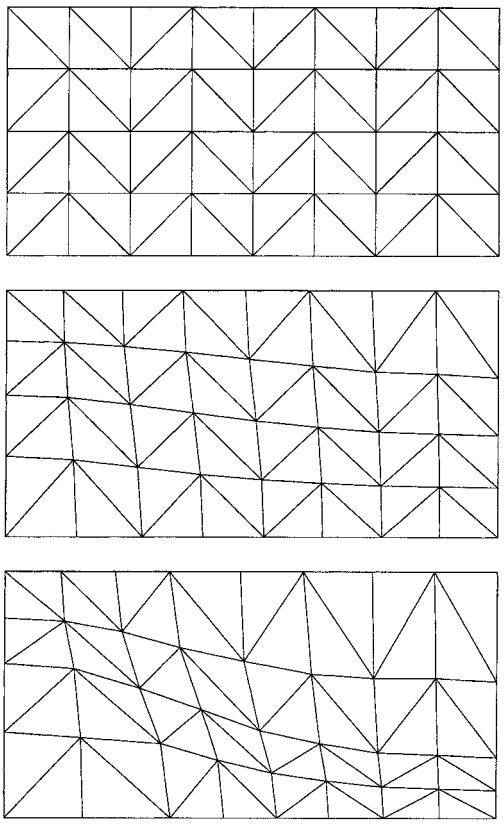

Fig. 14. Initial mesh (top), mesh at onset of plastification (center), and final mesh (bottom).

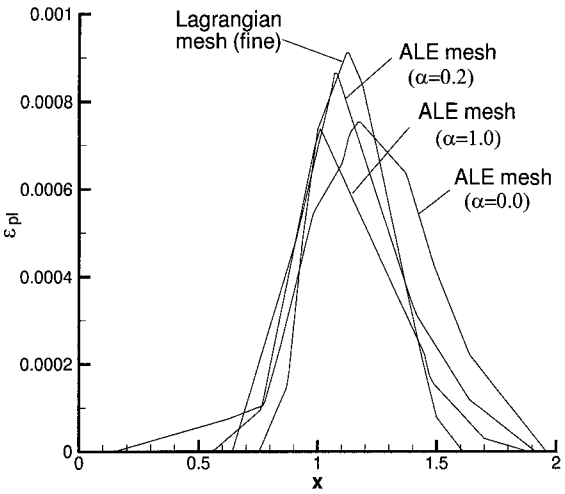

Fig. 15. Profiles of equivalent plastic strain along y x for different values of α.

compared to the coarse Lagrangian mesh (cf. Fig. 6) a much better solution has been achieved with the same number of elements. For a better comparison between the two Lagrangian solutions and the ALE solution, profiles of the equivalent plastic strain along the line y x and along the line x 3 (see Fig. 1) have been plotted in Figs 12 and 13, respectively. It can be con cluded that the ALE solution gives a good approxi mation of the peak values of the equivalent plastic strain, as well as of the width of the yield lines. To in vestigate the effect of carrying out remeshing in both the elastic and the plastic stage, subsequent meshes have been plotted in Fig. 14. At the onset of plastification (at load level $0.7 \times$ ultimate load level) el ements have already been moved according to the

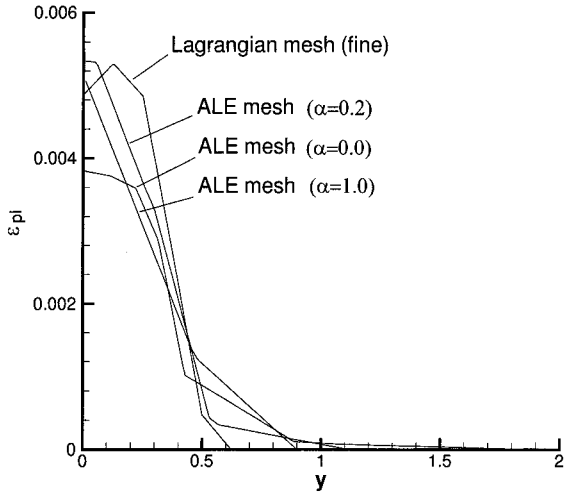

Fig. 16. Profiles of equivalent plastic strain along x 3 for different values of α.

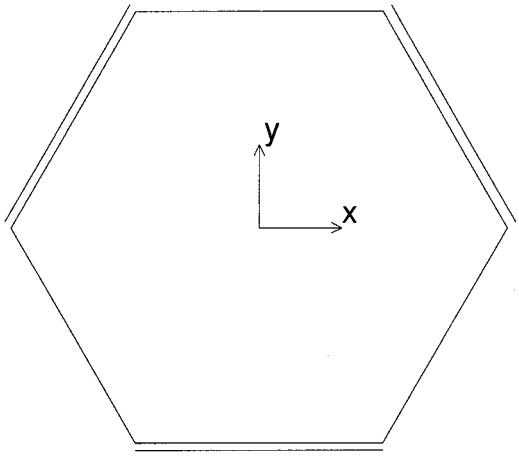

Fig. 17. Hexagonal plate problem statement.

yield lines that are to be formed. Since $\alpha = 0.2$, relatively little remeshing is carried out in the elastic stage, but the forming of the yield lines is not delayed. When remeshing is only performed in the elastic stage ($\alpha = 1.0$) or only in the plastic stage ($\alpha = 0.0$), results are obtained as shown in Figs 15 and 16, which show the profiles of the equivalent plastic strain along $y = x$ and along $x = 3$, respectively. It can be seen that results obtained with $\alpha = 0.2$ are better than with $\alpha = 0.0$ or $\alpha = 1.0$. Both the width of the yield line and the peak value of the equivalent plastic strain are predicted best when remeshing is carried out in the elastic stage as well as in the plastic stage. Especially in the case where $\alpha = 0.0$ inferior results are shown. Here, the yield line emerging from the sample's corners has shifted compared to the fine Lagrangian mesh, and the yield line at the sample's center is underestimated.

5.2. Hexagonal plate

The second example is a hexagonal plate, simply supported along three non adjacent sides (see Fig. 17). Each side has a length of 4 m. The plate thickness is 10 cm, while the same material set as for the first example has been used. A uniform load equal to 169 kN/m^2 has been applied, which is slightly smaller than the load level at which total collapse occurs. Yield lines start to form at the free edges, and propagate towards the center of the plate with increasing load level. Figs 18–20 show contours of the equivalent plastic strain for a Lagrangian mesh of 1538 elements, a Lagrangian mesh of 96 elements and an ALE mesh of 96 elements, respectively. Again, we desire an element size $\Omega_{des} = 0.04\ m^2$ for $\epsilon_{pl} = 0.001$. The initial element size $\Omega_{init} \approx 0.433\ m^2$, therefore according to Eq. (17) $a > 16$ (with $\alpha = 0.2$). We have taken $a = 25$. From the contour plots it can be concluded that 96 elements is too low a number when a Lagrangian analysis is car

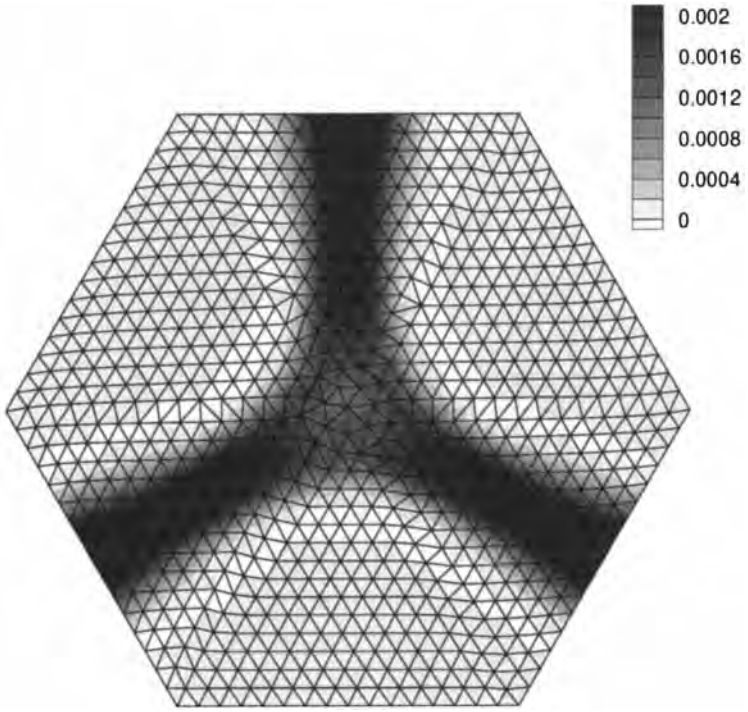

Fig. 18. Contour plot of equivalent plastic strain, Lagrangian, 1538 elements.

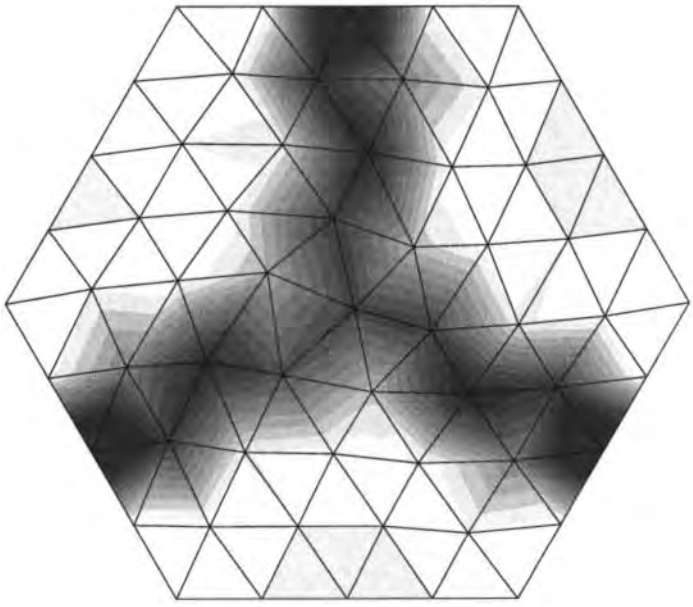

Fig. 19. Contour plot of equivalent plastic strain, Lagrangian, 96 elements.

ried out. Compared to the fine mesh solution of Fig. 18, the yield line pattern is very irregular. The slight distortion of the mesh highly influences the yield line pattern, while the forming of the yield lines is delayed by the too large sizes of the finite elements. Furthermore, the yield lines have not propagated towards the center of the plate. On the other hand, with the ALE algorithm, the 96 element mesh predicts a yield line pattern similar to the fine Lagrangian mesh. It can be seen that the mesh has been orientated along the yield lines, thus avoiding the strong irregula rities that occurred with the Lagrangian mesh. Further, the yield lines have fully developed. In Fig. 21, profiles of the equivalent plastic strain along the line y 2.5 m have been plotted. This figure shows in more detail the influence of the mesh distortion on the coar ser Lagrangian mesh, and the aligning according to the yield lines exhibited by the ALE solution.

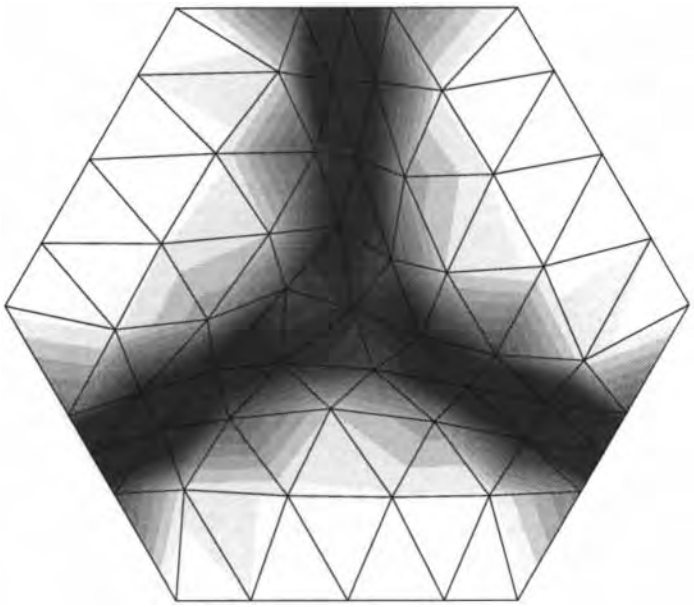

Fig. 20. Contour plot of equivalent plastic strain, ALE, 96 elements.

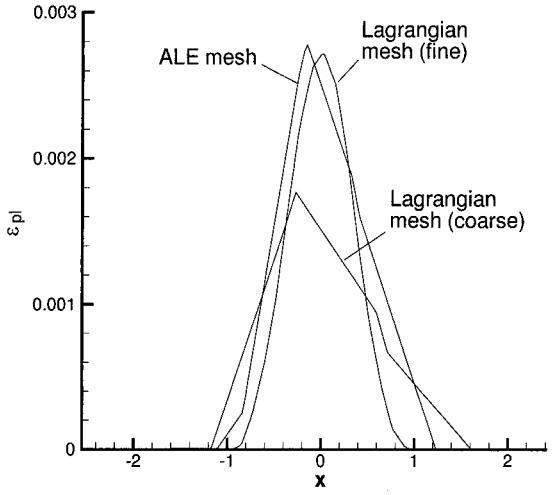

Fig. 21. Profiles of equivalent plastic strain along y 2.5.

5.3. Rectangular plate with eccentric square hole

The last example deals with a rectangular plate with an eccentric square hole. All sides are simply sup ported, and the dimensions are shown in Fig. 22. A uniform load equal to 125 kN/m^2 has been applied. The plate thickness reads 5 cm and the material set from the previous examples has been taken. Lagrangian analyses have been carried out using 3714 and 400 elements, as well as an ALE analysis with 400 elements. With Ω_{des} 0.04 m^2 for ϵ_{pl} 0.001 and $\Omega_{init} \approx 0.11$ m^2 the ALE remesh parameters have been taken as a 5 and α 0.2. The contour plots of the equivalent plastic strain are shown in Figs 23 25. Compared to the fine Lagrangian mesh, the coarse Lagrangian mesh has difficulties capturing the main yield lines departing from the upper left corner and the lower left corner towards the center of the plate. On the other hand, the ALE solution does not show this deficiency. Elements are being aligned along the yield lines during the remeshing procedure. A closer inspec tion of the upper left yield line is shown in Fig. 26. Here, an excellent agreement between the Lagrangian solution with the fine mesh and the ALE solution can be seen. Yet, due to the dominance of the yield lines in the left part of the plate, nodes around the square hole are attracted towards the left. Together with the fixed connectivity of the elements, this has resulted in very large aspect ratios of the elements around the corners of the square hole. This may influence the quality of the solution locally. However, since the major import ance is put on the description of the main yield lines that appear at the left part of the plate, this locally poor quality is acceptable.

6. Conclusions

Plates are common structure types in engineering practice. The failure analysis of plates requires robust and efficient numerical tools. Plasticity models have proven to be very suitable for the description of the failure behaviour of plates. The description of the yield line pattern that occurs with plastic failure of plates is of major importance. However, the yield line pattern heavily depends on the geometry of the plate, as can be seen from both analytical and numerical calcu lations. To capture the yield line pattern correctly, usually very fine meshes must be used. Yet, this poses severe requirements on the computer capacities. To cir cumvent the use of these very fine meshes, mesh adap

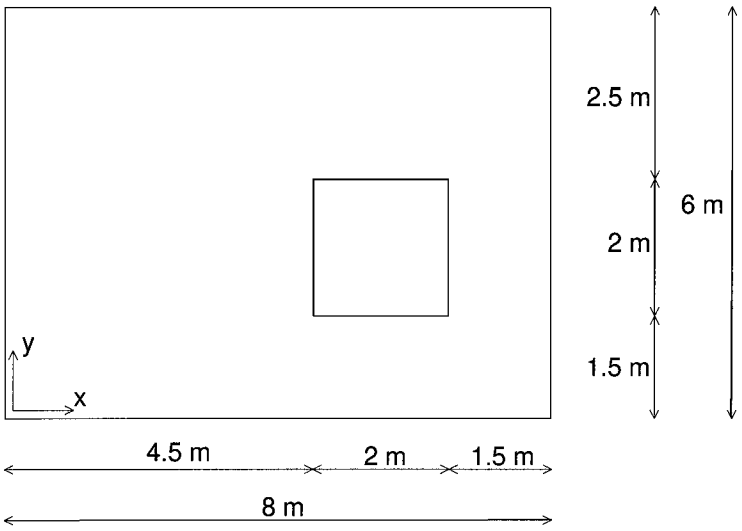

Fig. 22. Rectangular plate with square hole problem statement.

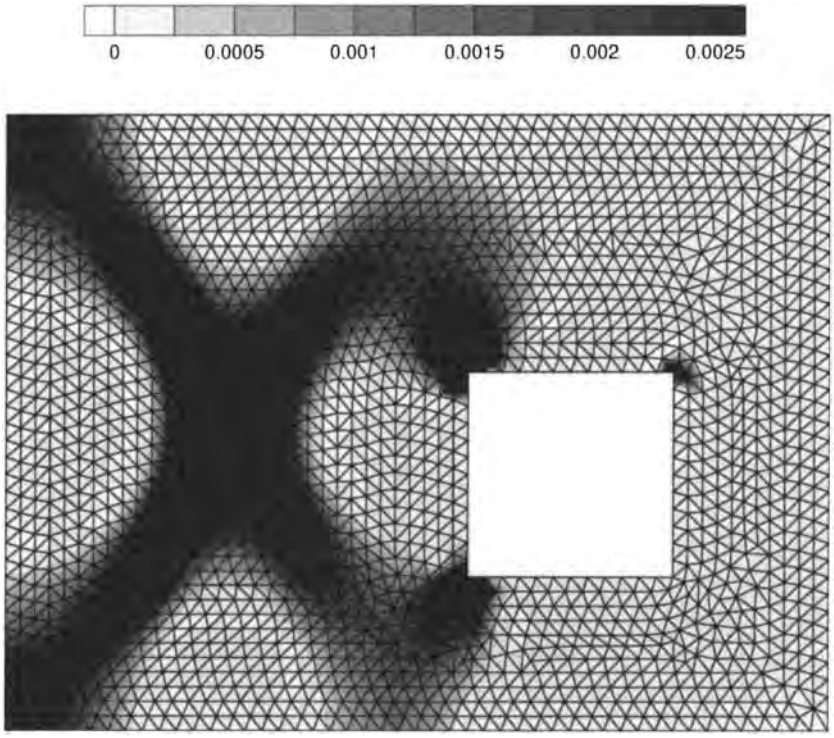

Fig. 23. Contour plot of equivalent plastic strain.

tion can be applied. In this study we have used the arbitrary Lagrangian Eulerian (ALE) technique as a continuous and automatic mesh adaptivity method. Remeshing is carried out during the computation such that the finite element description is automatically refined at the yield lines. Within an ALE formulation,

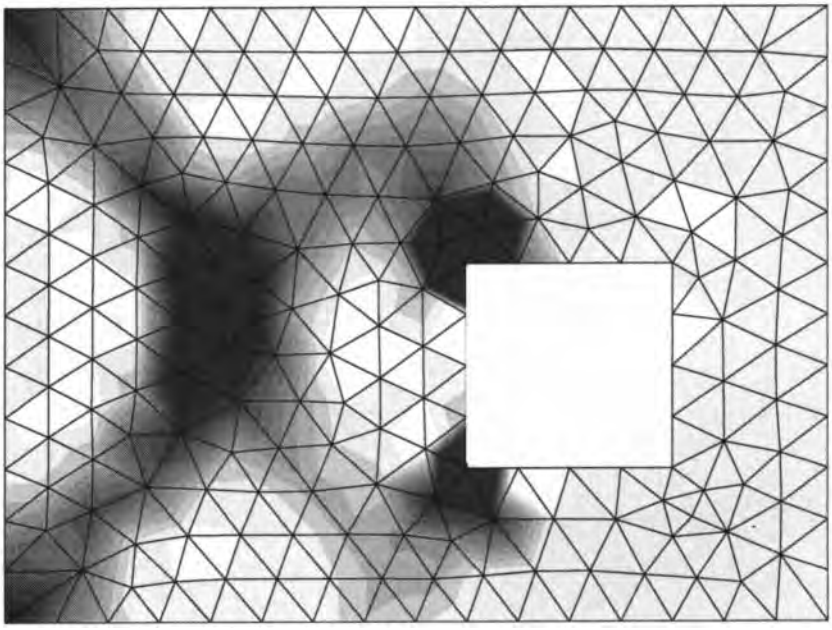

Fig. 24. Contour plot of equivalent plastic strain.

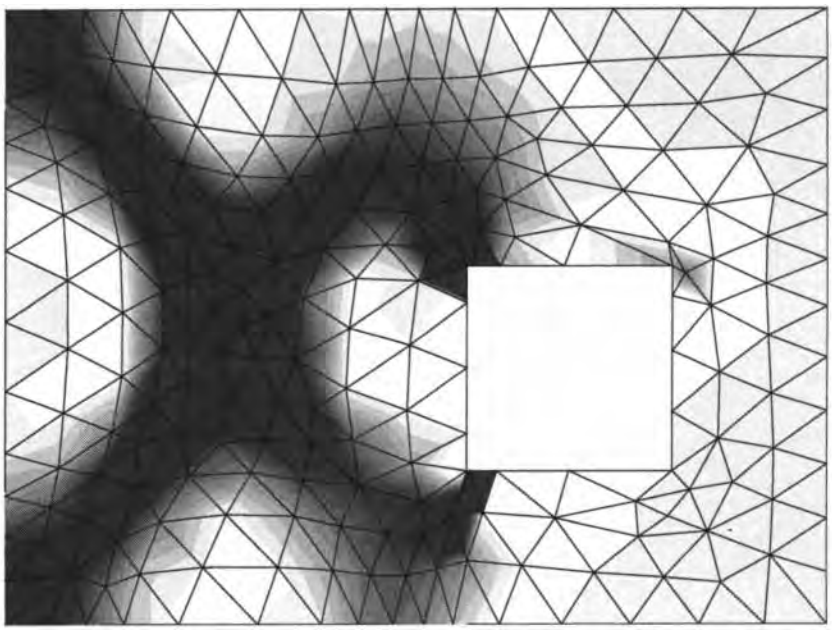

Fig. 25. Contour plot of equivalent plastic strain.

both the element connectivity and the number of applied elements remain constant throughout the analysis.

To be able to describe both newly appearing yield lines and already formed yield lines, we have formulated a remesh indicator that concentrates elements in zones which are close to yielding as well as in zones that are already plastified. Numerical analyses show that, with the ALE technique, yield lines can be described with an accuracy competitive with very fine standard Lagrangian meshes. If the same number of elements as in the ALE analyses are used within a Lagrangian formulation, the yield line pattern is heavily determined by the orientation of the mesh, and the proper propagation of the yield lines is delayed. These deficiencies are overcome with the ALE technique. Therefore, the ALE technique allows for solutions that are both accurate and cheap (cheap in terms of computer time), which makes this approach attractive for use in large scale computations.

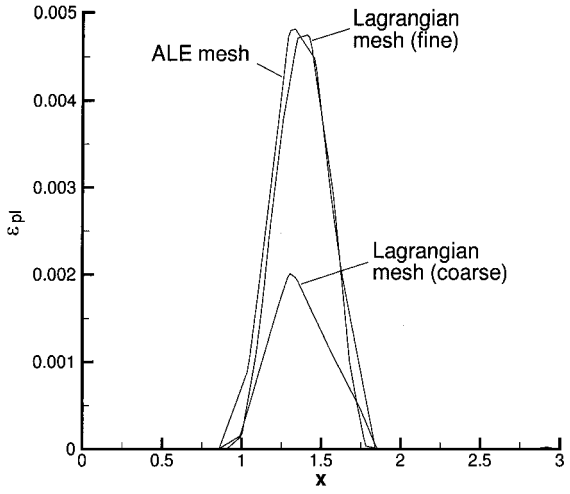

Fig. 26. Profiles of equivalent plastic strain along $y \quad x + 3$.

Acknowledgements

The first author would like to thank Pedro Díez Mejía for fruitful discussions, and the HCM network ERBCHRX CT94 0629 for financial support. Furthermore, we gratefully acknowledge the Commissariat à l'Énergie Atomique, France, for the availability of the finite element code Castem2000 for this research.

Appendix A

A.0.1. The discrete Kirchhoff triangle

The discrete Kirchhoff triangle (DKT) that is used throughout this work combines a rapid convergence and a robust behaviour with relatively low computer costs [1, 13].

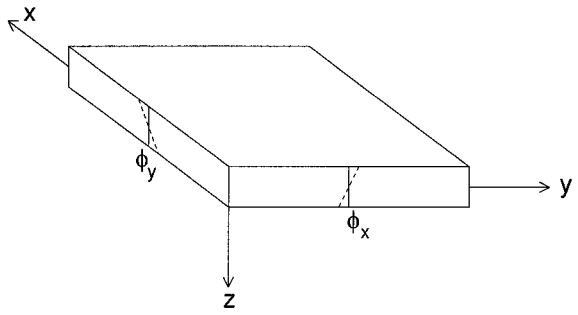

Fig. 27. Sign convention for plate rotations.

The thin shell assumption is made, i.e. it is assumed that the transverse shear deformations γ_{xz} and γ_{yz} van ish:

$$\begin{bmatrix} \gamma_{xz} \\ \gamma_{yz} \end{bmatrix} \quad \begin{bmatrix} \phi_x \\ \phi_y \end{bmatrix} + \begin{bmatrix} \dfrac{\partial w}{\partial x} \\ \dfrac{\partial w}{\partial y} \end{bmatrix} \quad \begin{bmatrix} 0 \\ 0 \end{bmatrix} \tag{18}$$

where ϕ_x and ϕ_y are the rotations of the normal along the x and y axis, respectively, and w is the normal dis placement of the plate (i.e. in the z direction), see Fig. 27.

In discrete Kirchhoff theory, the Kirchhoff assump tion [Eq. (18)] is only fulfilled at discrete points. Normally, point collocation is used. The resulting equations are then used to reduce the number of nodal unknowns [1]. As a consequence, the DKT element has only three unknowns per node, namely w, ϕ_x, and ϕ_y.

References

[1] Zienkiewicz OC, Taylor RL. The finite element method. In: Solid and fluid mechanics, dynamics and non linear ity, volume 2. 4th ed. Berkshire: McGraw Hill, 1991.

[2] Johansen KW. Yield line theory. London: Cement and Concrete Association, 1962.

[3] Wood RH. Plastic and elastic design of slabs and plates. London: Thames and Hudson, 1961.

[4] Belytschko T, Kennedy JM. Computer methods for sub assembly simulation. Nuclear Engineering and Design 1978;49:17 38.

[5] Donéa J. Arbitrary Lagrangian Eulerian finite element methods. In: Belytschki T., Hughes T.J.R., eds. Computational methods for transient analysis, ch. chap. 10. New York: Elsevier, 1983.

[6] Hughes TJR, Liu WK, Zimmermann TK. Lagrangian Eulerian finite element formulation for incompressible viscous flows. Computer Methods in Applied Mechanics and Engineering 1981;29:329 49.

[7] Huerta A, Liu WK. Viscous flow with large free surface motion. Computer Methods in Applied Mechanics and Engineering 1988;69:277 324.

[8] Liu WK, Belytschko T, Change H. An arbitrary Lagrangian Eulerian finite element method for path dependent materials. Computer Methods in Applied Mechanics and Engineering 1986;58:227 46.

[9] Schreurs PJG, Veldpaus FE, Brekelmans WAM. Simulation of forming processes, using the arbitrary Eulerian Lagrangian formulation. Computer Methods in Applied Mechanics and Engineering 1986;58:19 36.

[10] Huétink J, Vreede PT, Van der Lugt J. Progress in mixed Eulerian Lagrangian finite element simulation of forming processes. International Journal for Numerical Methods in Engineering 1990;30:1441 57.

[11] Pijaudier Cabot G, Bodé L, Huerta A. Arbitrary Lagrangian Eulerian finite element analysis of strain localization in transient problems. International Journal for Numerical Methods in Engineering 1995;38:4171 91.

[12] Bodé L. Stratégies numériques pour la prévision de la ruine des structures du génie civil. Dissertation, E.N.S. de Cachan/CNRS/Université Paris, 1994.

[13] Prat M., Bisch Ph, Millard A., Mestat Ph, Pijaudier Cabot G. La modélisation des ouvrages. Paris: Hermès, 1995.

[14] Huerta A, Casadei F. New ALE applications in non lin ear fast transient solid dynamics. Engineering Computations 1994;11:317 45.

[15] Askes H. Mesh adaptivity methods: the ALE technique for localisation. Technical report 03.21.1.31.09, Delft University of Technology, 1997.

[16] Rodríguez Ferran A, Casadei F, Huerta A. ALE stress update for transient and quasistatic processes. International Journal for Numerical Methods in Engineering 1998;43:241 62.

[17] Huerta A, Casadei F, Donéa J. ALE stress update in transient plasticity problems. In: Owen D.R.J., Oñate E., editors. Computational plasticity IV, fundamentals and applications. Swansea: Pineridge Press, 1995:1865 76.

[18] LeVeque RJ. Numerical methods for conservation laws. 2nd ed. Basel: Birkhauser, 1992.

[19] Sluys LJ, Cauvern M, de Borst R. Discretization influ ence in strain softening problems. Engineering Computations 1995;12:209 28.

[20] Huerta A, Pijaudier Cabot G. Discretization influence on the regularization by two localization limiters. ASCE Journal Engineering Mechanics 1994;120:1198 218.

[21] Askes H, Sluys LJ. A remeshing strategy for 3D crack propagation with a regularised continuum model. In: de Borst R, Bićanić N, Mang H, Meschke G, editors. Euro C 1998, Computational modelling of concrete structures. Rotterdam: Balkema, 1998:391 7.

[22] Rodríguez Ferran A, Askes H, Huerta A. Arbitrary Lagrangian Eulerian analyses of plastic failure in plates. In Idelsohn, SR, Oñate E, Dvorkin EN, editors. Fourth world congress on computational mech anics, new trends and applicaitons, CD ROM proceed ings. Barcelona:CIMNE, 1998..

[23] Castem2000, Manuel d'utilisation. Technical report 88/ 176, Laboratoire d'Analyse mécanique des Structures, Commissariat à l'Énergie Atomique, Saclay, France. 1988.